Stress and temperature dependence of stress relaxation ageing behaviour of an Al-Zn-Mg alloy

Fenggong Lyu[a,d,e], Yong Li[b,*], Zhusheng Shi[c,*], Xia Huang[a,d,e], Yuansong Zeng[a,d,e], Jianguo Lin[c]

[a]AVIC Manufacturing Technology Institute, Beijing 100024, China

[b]School of Mechanical Engineering and Automation, Beihang University, Beijing 100191, China

[c]Department of Mechanical Engineering, Imperial College London, London SW7 2AZ, UK

[d]Aeronautical Key Laboratory for Plastic Forming Technologies, Beijing 100024, China

[e]Beijing Key Laboratory of Digital Plasticity Forming and Equipment, Beijing 100024, China

* Corresponding author: liyong19@buaa.edu.cn (Y. Li)

zhusheng.shi@imperial.ac.uk (Z. Shi)

Abstract

The stress (from elastic to plastic) and temperature dependence of stress relaxation ageing (SRA) behaviour of an Al-Zn-Mg alloy, AA7B04-P, has been experimentally investigated in this study. A series of SRA tests have been carried out under various initial stress levels in both elastic and plastic regions and at different temperatures. Corresponding microstructural evolution during SRA has been characterised using transmission electron microscopy (TEM). It is found that increasing the initial stress and/or temperature enhance the stress relaxation in both elastic and plastic regions. The dislocation creep mechanism plays the dominant role at the investigated temperatures during SRA, with the stress exponent *n* ranging from 3 to 8, decreasing with increasing temperature. External stresses accelerate the coarsening of GP zones and η' precipitates and, when loaded to the plastic region, promote the formation of large rod-shaped η precipitates within 2 h of SRA tests, due to the high energy sites provided by dislocations from plastic loading. Yield strength shows a much higher sensitivity to the temperature than creep strain has during SRA tests. A temperature below 165 °C is suggested for SRA of AA7B04-P, so that a high stress relaxation level with less than 15% strength loss can be obtained after 16 h forming.

Keywords: Stress relaxation; Ageing; Al-Zn-Mg alloy; AA7B04; Precipitation; Creep age forming.

Highlights:

- The different SRA behaviour in elastic and plastic regions can be appropriately divided by 0.01% offset stress
- Total relaxed stress increases linearly with initial stress/strain in elastic region
- Dislocation dominated mechanism controls SRA of AA7B04 between 155 and 175 °C
- Plastic loading highly accelerates the formation of large rod-shaped η precipitates
- Yield strength has a higher sensitivity to temperature than creep strain during SRA

1. Introduction

The 7000 series Al-Zn-Mg alloys provide the highest strength of all aluminium alloys, and are widely used for the structural panels in the aerospace industry, such as the upper wing skins, stringers and stabilisers [1]. Creep age forming (CAF) process, which integrates the thermally activated creep deformation and artificial ageing to concurrently form and strengthen aluminium alloy products, has been reported as an advanced forming technology to manufacture these large panels [2]. Due to the increasing demand of high performance aircrafts with low emission, integrally stiffened panels are becoming more and more popular for aeronautic products, such as upper wing stiffened panels with Al-Zn-Mg alloys reported by Dursun and Soutis [3], which have higher performance with lower weight when compared with conventional structures by connecting formed skins and stiffeners through welding or riveting [4]. Holman [5] has been reported that the conventional large/extra-large skins in the airplanes, such as wings, can be manufactured by CAF process in the elastic region, and thus, many studies focused on investigating [6] and modelling [7] the creep-ageing behaviour of aluminium alloys in the elastic region to guide potential CAF applications. However, Lyu et al. [8] have reported that it is easy to reach plastic deformation region when the stiffened panels are loaded to the same shape of skins for CAF manufacture, and the current knowledge and models developed for creep-ageing in the elastic region may not be able to provide an accurate prediction of the springback of stiffened panels after CAF. Hence, a comprehensive understanding of the creep-ageing behaviour under different stress levels in both elastic and plastic regions becomes necessary for advanced industrial applications of CAF process.

Creep-ageing tests (holding a constant stress at an elevated temperature) is commonly used to obtain the creep-ageing behaviour of aluminium alloys in the elastic region, due to its low requirement on the experimental instruments [9]. The creep-ageing behaviour of various heat treatable aluminium alloys in the elastic region has been widely investigated, such as Al-Cu-Mg by [10], Al-Zn-Mg by [11] and Al-Cu-Li by [12], and corresponding modelling techniques have also been developed by [13]. It is generally believed that the stress relaxation during CAF mainly comes from the thermally activated creep strains [14]. Hence, the developed creep-ageing models have been widely used to assist the springback prediction of the formed components after CAF by implementing them into finite element (FE) simulations with different commercial solvers, such as PAM-STAMP [15] and ABAQUS [16]. However, when the material is loaded to the plastic region, creep-ageing tests are no longer appropriate to

characterise the creep strain evolutions in the alloy, and stress relaxation ageing (SRA) tests (holding a constant strain at an elevated temperature) become a more suitable choice.

The stress relaxation behaviour of aluminium alloys at artificial ageing temperatures has been reported to show a three-stage behaviour, including the initial stage with high stress relaxation rates, subsequent transition stage and final equilibrium stage [17]. Chen et al. [18] investigated the stress relaxation behaviour of an Al-Zn-Mg alloy in the elastic region during CAF and employed the creep stress exponent analysis method to characterise the stress relaxation mechanisms of the alloy at different stress relaxation stages. The same method has also been adopted by Zhan et al. [19] for stress relaxation analysis of an AA2219 alloy. Rong et al. [20] have investigated the SRA behaviour of an Al-Mg-Si alloy (AA6082) in both elastic and plastic regions, and reported that a much higher level of stress relaxation occurs when loaded to the plastic region, which cannot be directly explained by conventional creep stress exponent analysis. A possible reason has been proposed as the decrease of threshold stress in the material due to the initial dislocations introduced when loaded to the plastic region. Related studies covering both elastic and plastic loading conditions for SRA behaviour of Al-Zn-Mg alloys are still not available currently.

In addition to the stress levels, temperature affects the precipitation progress and is a key factor to determine the stress relaxation and ageing behaviour of aluminium alloys during CAF. A proper temperature is required to achieve a satisfactory yield strength after ageing, otherwise, the resultant precipitate types and distributions may be detrimental to the strength of the alloys [21]. A high temperature can facilitate the creep deformation of the alloys, but too high a temperature may lead to the tertiary creep stage in a short time, which should be avoided in CAF applications [22]. Additionally, different temperatures may also introduce different effects on the SRA behaviour in the elastic and plastic regions. Hence, a thorough understanding of the stress and temperature dependence of SRA behaviour of Al-Zn-Mg alloys is important to provide a useful guidance for choosing proper processing parameters for CAF applications of the alloys.

In this study, the stress and temperature dependence of the SRA behaviour of an Al-Zn-Mg alloy, AA7B04, has been comprehensively investigated. SRA tests have been carried out under various initial stress levels in both elastic and plastic regions and at three selected temperatures. Microstructural observations of some stress relaxation aged samples have been performed using transmission electron microscopy (TEM), to support the detailed investigation of the

temperature and stress effects on SRA behaviour of the Al-Zn-Mg alloy and the analysis of corresponding strengthening and deformation mechanisms.

2. Experiments

2.1 Materials and heat treatments

The material used in this study is an Al-Zn-Mg alloy, AA7B04, whose main chemical composition is Al-5.97Zn-2.48Mg-1.51Cu (wt%). The as-received material is with a special initial temper, designated as AA7B04-P in this study, which had undergone 1 h solution heat treatment at 470 °C, water-quenching, 2% pre-stretching and a single step artificial ageing at 115 °C for 8 h, as illustrated in Fig. 1.

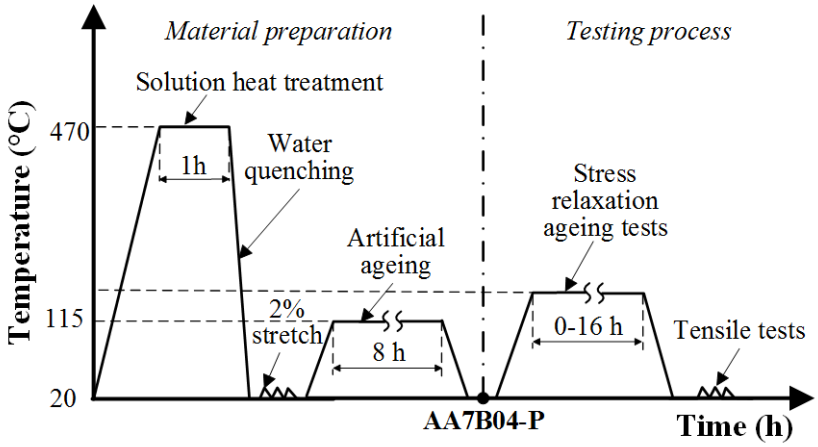


Fig. 1. Thermal history of AA7B04-P material and subsequent SRA and tensile tests.

2.2 Stress relaxation ageing and tensile tests

Dog-bone specimens with a gauge length of 50 mm and radius of 8 mm were machined from the as-received thick plate. The samples were machined along the direction perpendicular to its rolling direction for SRA and tensile tests, as the main deformation occurs in this direction in CAF applications, such as wing skins of aircrafts. SRA tests were carried out at three ageing temperatures: 155, 165 and 175 °C, which are potential temperatures for CAF of Al-Zn-Mg alloys [23]. Preliminary tensile tests of AA7B04-P were performed at these three temperatures to determine the initial stress levels in both elastic and plastic regions for SRA tests. The 0.01% ($\sigma_{0.01\%}$) and 0.2% ($\sigma_{0.2\%}$) offset yield strengths and corresponding strain values of $\varepsilon_{0.01\%}$ and $\varepsilon_{0.2\%}$, and Young's modulus of the material at the test temperatures are listed in Table 1. As the creep strains generated during CAF are very small, e.g. 0.25% after 20 h creep-ageing of AA7B04-T651 under 270 MPa at 140 °C [8], $\sigma_{0.2\%}$ used for engineering applications may ignore too many plastic strains when considering the small accumulated creep strains. Hence,

$\sigma_{0.01\%}$ was used to divide the elastic and plastic regions of the material during loading in this study, and based on which, SRA tests were carried out under six initial stress/strain levels at each temperature, three in the elastic region and three in the plastic region, as listed in Table 2. In addition, in order to investigate the evolution of yield strength of the material during SRA tests, interrupted tests with different time durations, including 2, 4, 8 and 16 h, were carried out, also listed in Table 2. Room temperature tensile tests were performed on all specimens after SRA tests and the $\sigma_{0.2\%}$ value of these tested specimens were calculated to guide further industrial applications.

Table1. Main mechanical properties of AA7B04-P material at different temperatures.

Temperature	$\sigma_{0.01\%}/\varepsilon_{0.01\%}$	$\sigma_{0.2\%}/\varepsilon_{0.2\%}$	Young's modulus (E)
155 ºC	355 MPa/0.564%	406 MPa/0.830%	64.8 GPa
165 ºC	325 MPa/0.529%	387 MPa/0.803%	62.5 GPa
175 ºC	296 MPa/0.478%	369 MPa/0.765%	58.9 GPa

Table 2. Temperature, initial stress/strain level and duration for SRA tests.

Temperature	**Initial stress/strain levels (MPa/%)**	**Testing time (h)**
155 ºC	Elastic: 250/0.386, 300/0.463 and 350/0.540	2, 4, 8 and 16
	Plastic: 370/0.591, 390/0.715 and 410/0.940	
165 ºC	Elastic: 200/0.320, 250/0.400 and 300/0.480	2, 4, 8 and 16
	Plastic: 350/0.592, 370/0.663 and 390/0.916	
175 ºC	Elastic: 150/0.255, 200/0.340 and 250/0.424	2, 4, 8 and 16
	Plastic: 300/0.512, 350/0.667 and 370/0.808	

Both SRA and tensile tests were executed on an Instron 5584 machine with an affiliated furnace which provides the high temperature environment for SRA tests. The temperature during tests was controlled within $\pm$ 3 ℃. During SRA tests, the specimens were loaded to the designated strain levels after the required temperature had been achieved, the strain recorded by an Instron dynamic extensometer 2602-601 was then held constant for a specific time duration. The subsequent tensile tests were carried out under a quasi-static condition with a strain rate of 10^{-4} s^{-1}.

2.3 Microstructural examination

Selected specimens were examined using TEM to investigate the effect of different stress and temperature conditions on precipitation behaviour of the alloy. The selected specimens

include the as-received material, the specimens stress relaxation aged (SRAed) for 16 h at 165 °C under different initial stress levels (elastic region: 0, 200 and 300 MPa; plastic region: 370 MPa), and the specimens SRAed for 16 h under 370 MPa at different temperatures (155, 165 and 175 °C). Samples were cut with a low-speed cutting saw, mechanically thinned down to 100 μm. 3 mm diameter discs were then prepared and twin-jet electropolished with a 20% perchloric acid alcohol solution in methanol maintained at −20 °C and 20 V. The prepared samples were examined with a FEI Tecnai G2 F20 TEM. The quantified data of precipitates were obtained by analysing three TEM images from different locations of the same sample.

3. Results

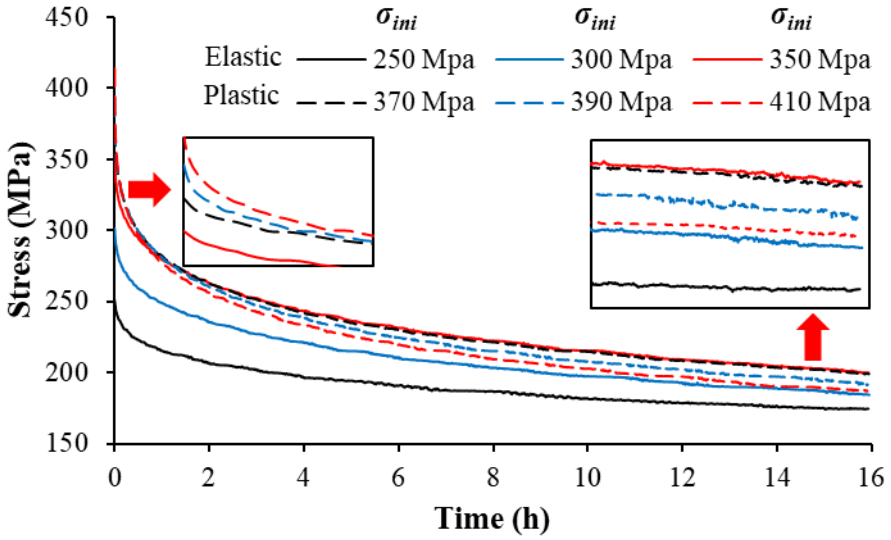
3.1 Stress relaxation behaviour

3.1.1 Stress relaxation curves

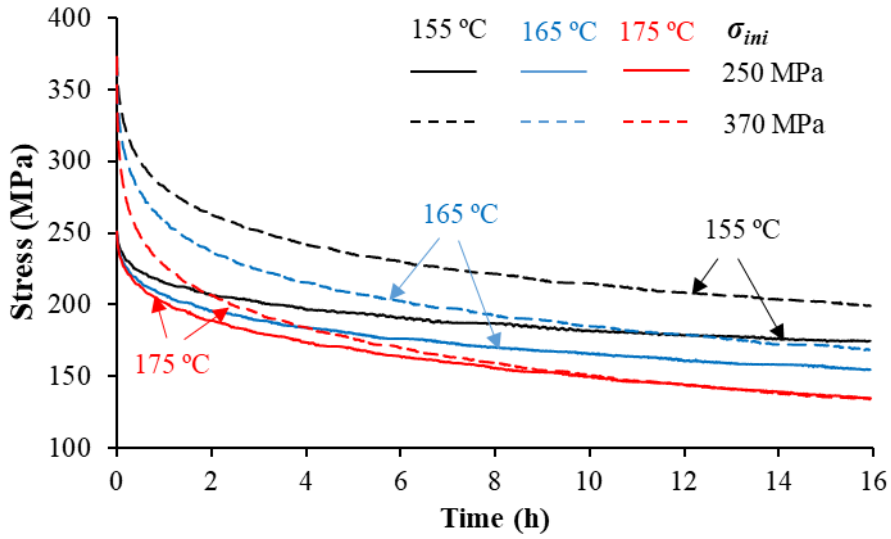
The stress relaxation curves of AA7B04-P under the tested initial stress levels and temperatures are shown in Fig. 2. All the stress relaxation curves under initial stress levels in both elastic and plastic regions show a similar trend, decreasing sharply at the initial stage, with a monotonously decreasing speed afterwards, until reaching a comparatively stable level. The same trend of stress relaxation curves has been widely reported in aluminium alloys [19], which has been explained by the quick propagation and accumulation of dislocations at the beginning of stress relaxation, and the equilibrium of accumulation and recovery of dislocations at the later stage of stress relaxation. However, the stress relaxation levels with initial stresses in the elastic and plastic regions show different behaviour. When the material is initially loaded in the elastic region ($\sigma_{ini} < \sigma_{0.01\%}$ in this study), a higher initial stress (σ_{ini}) leads to a larger remaining stress (σ_r) after 16 h stress relaxation tests, while except for the very beginning, an opposite trend is seen when loaded in the plastic region ($\sigma_{ini} \geq \sigma_{0.01\%}$ in this study), where a lower σ_r value exists for a higher σ_{ini} level. A similar phenomenon has been reported during stress relaxation of an Al-Mg-Si alloy [20], although the 0.2% proof stress ($\sigma_{0.2\%}$) was used as the yield point., and the threshold stress for creep of the alloy has been indicated as a key factor for this phenomenon, as threshold stress may decrease when loaded to the plastic region due to the high movability of dislocations, and thus leading to the higher relaxed stress levels after the tests.

Fig. 2(b) shows the temperature effect on stress relaxation behaviour at two selected initial stress levels: 250 MPa in the elastic region and 370 MPa in the plastic region. It shows that with the same initial stress level and the same testing time, more stresses are relaxed at higher

temperatures. This is true in both elastic and plastic regions, as a higher temperature provides more energy for the propagation of dislocations, leading to easier dislocation movements and higher resultant relaxed stresses [24].



(a)



(b)

Fig. 2. Stress relaxation behaviour of AA7B04-P: (a) under different initial stress levels at 155 ºC and (b) at different temperatures (solid lines: elastically loaded; dashed lines: plastically loaded).

3.1.2 Maximum relaxed stresses

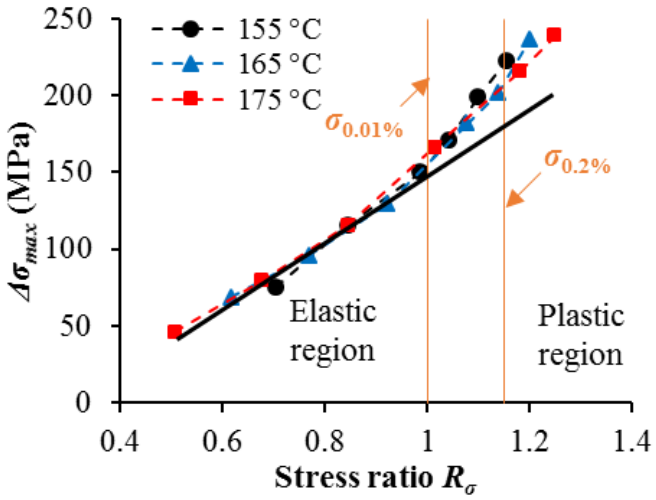
In order to directly compare the stress relaxation level of AA7B04-P at different testing conditions, Fig. 3 plots the variations of the maximum relaxed stress values after 16 h SRA tests ($\Delta\sigma_{max} = \sigma_{ini} - \sigma_r$) against the normalised applied stress and strain levels. The

normalised applied stress and strain, or the stress ratio R_σ and strain ratio R_ε, are defined as the ratios of the initial values to the critical values at the 0.01% offset yield condition listed in Table 1:

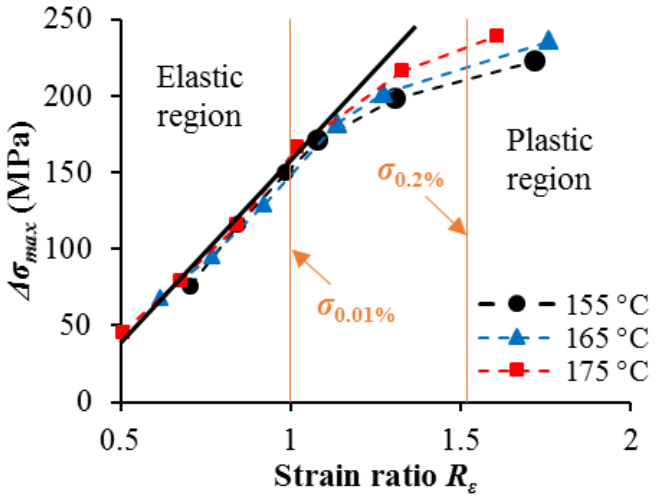
$$R_\sigma = \sigma_{ini}/\sigma_{0.01\%} \quad (1)$$

$$R_\varepsilon = \varepsilon_{ini}/\varepsilon_{0.01\%} \quad (2)$$

in which ε_{ini} is the initial strain, $\varepsilon_{0.01\%}$ is the strain corresponding to 0.01% offset stress. When R_σ or R_ε is larger than 1, the material is loaded in the plastic region defined by $\sigma_{0.01\%}$. The line representing the normalised level of the 0.2% offset stress ($\sigma_{0.2\%}$) is also plotted in Fig. 3.



(a)



(b)

Fig 3. Variations of maximum stress drop ($\Delta\sigma_{max} = \sigma_{ini} - \sigma_r$) after 16 h SRA tests under different (a) stress ratios ($R_\sigma = \sigma_{ini}/\sigma_{0.01\%}$) and (b) strain ratios ($R_\varepsilon = \varepsilon_{ini}/\varepsilon_{0.01\%}$) at indicated temperatures.

When the yield condition is defined by $\sigma_{0.01\%}$, it can be seen from Fig. 3(a) that in the elastic region, $\Delta\sigma_{max}$ increases almost linearly with the stress ratio R_σ and has a similar relationship for all three test temperatures. Because of the linear correspondences between stress and strain in the elastic region, a similar phenomenon also exists between $\Delta\sigma_{max}$ and R_ε, as shown in Fig. 3(b). These results indicate a same stress relaxation mechanism of the material in the test temperature range, which will be discussed in Section 4.2. When loaded to the plastic region, the linear relationship between $\Delta\sigma_{max}$ and R_σ (or R_ε) no longer exists. $\Delta\sigma_{max}$ experiences a higher increasing rate with R_σ in the plastic region than that in the elastic region, as shown in Fig. 3(a). Meanwhile, $\Delta\sigma_{max}$ increases with a decreasing rate and tends to achieve a saturate level with increasing strain ratio in the plastic region, as shown in Fig. 3(b), which is due to the fact that the applied stress σ_{ini} cannot increase infinitively and will achieve the highest level at a specific strain value in the flow stress curve. These phenomena could be explained by the dislocation evolutions, as the initial dislocations from plastic loading which facilitate stress relaxation of the material will also reach a saturate level at high plastic strain levels due to the combined effects of accumulation and recovery [25, 26]. In addition, when loaded to the plastic region, a higher testing temperature leads to a slightly larger $\Delta\sigma_{max}$ value at the same strain ratio in Fig. 3(b), which is related to the temperature effect on dislocation evolutions and will be discussed in Section 4.2.

However, if the yield condition is defined by the engineering proof stress $\sigma_{0.2\%}$, it can be seen in Fig. 3 that the consistent linear relationship between $\Delta\sigma_{max}$ and R_σ (or R_ε) is lost beyond $\sigma_{0.01\%}$. The results indicate that the conventional $\sigma_{0.2\%}$ proof stress is not a good representation of the yield point for stress relaxation behaviour study, as some initial plastic strains and dislocations have already been introduced when loaded to $\sigma_{0.2\%}$, whose contributions to the stress relaxation progress of aluminium alloys cannot be ignored, as indicated by Fig. 3.

3.1.3 Creep strains

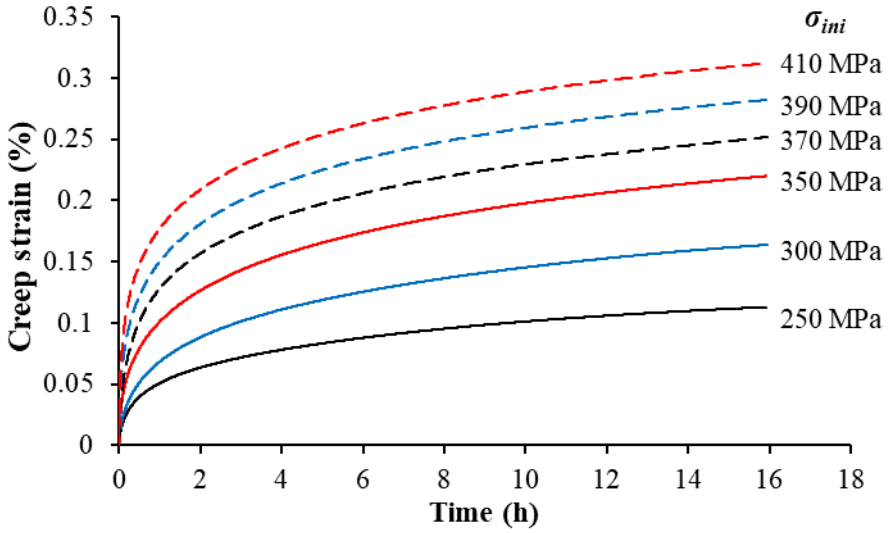
It is known that the stresses relaxed during SRA tests are mainly due to part of elastic strains in the loaded material being converted to creep strains [9]. Hence, the total strain (ε_t) in the material during stress relaxation consists of three parts: elastic strain (ε_e), initial plastic strain if loaded to the plastic region (ε_p), and creep strain (ε_c):

$$\varepsilon_t = \varepsilon_e + \varepsilon_p + \varepsilon_c. \quad (3)$$

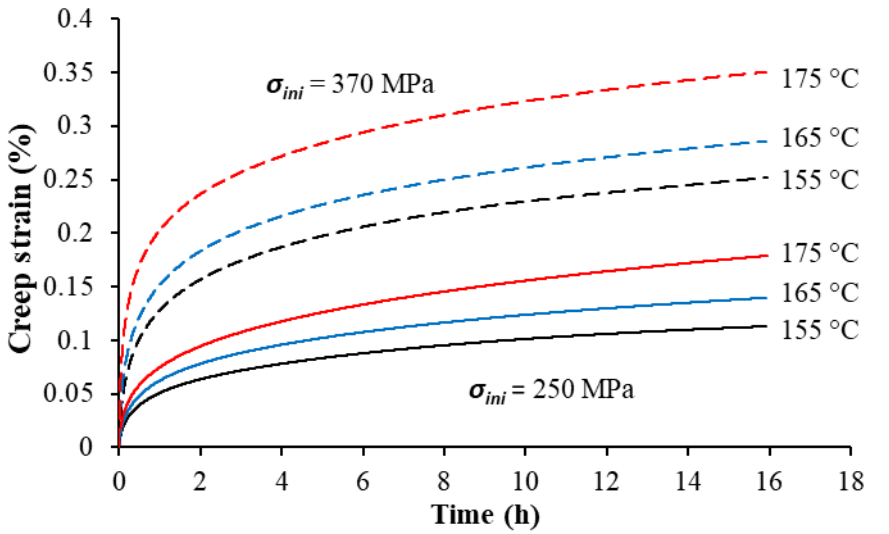
As the total strain and initial plastic strain are constant during SRA tests, the evolution of creep strain rate ($\dot{\varepsilon}_c$) then can be calculated by the changing elastic strains ($\dot{\varepsilon}_e$), as:

$$\dot{\varepsilon}_c = -\dot{\varepsilon}_e = -\frac{\dot{\sigma}}{E}. \quad (4)$$

The evolution of creep strains during SRA tests were calculated by integrating Eq. (4) with respect to time, and corresponding results under different initial stress levels and temperatures are shown in Fig. 4. A higher applied stress results in a higher creep strain rate, leading to the larger creep strain values shown in Fig. 4(a). Under the same applied stress level, a higher temperature leads to larger creep strains after SRA tests. According to Eq. (4), $\dot{\varepsilon}_c$ is proportional to $\dot{\sigma}$. The stress relaxation rate decreases sharply initially, therefore the initial high level of creep strain rate also decreases sharply at the initial stage, followed by a progressively decreasing speed, until approaching 0 with a stable remaining stress.



(a)



(b)

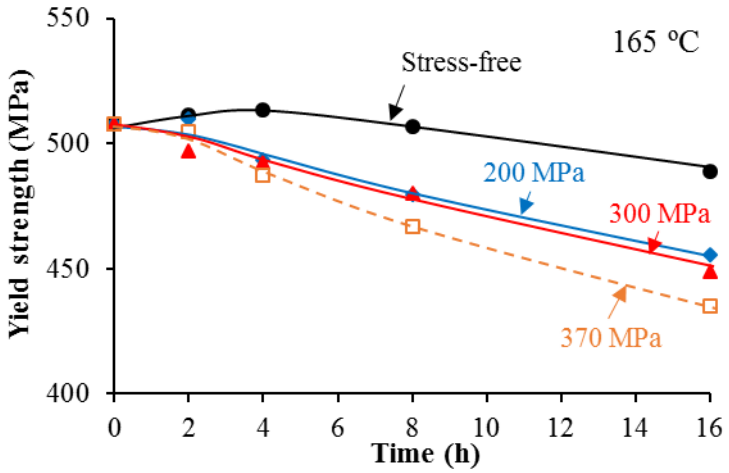
Fig. 4. Creep strains during SRA tests of AA7B04-P: (a) under different initial stress levels at 155 ºC and (b) at different temperatures (solid lines: elastically loaded; dashed lines: plastically loaded).

3.2 Age hardening behaviour

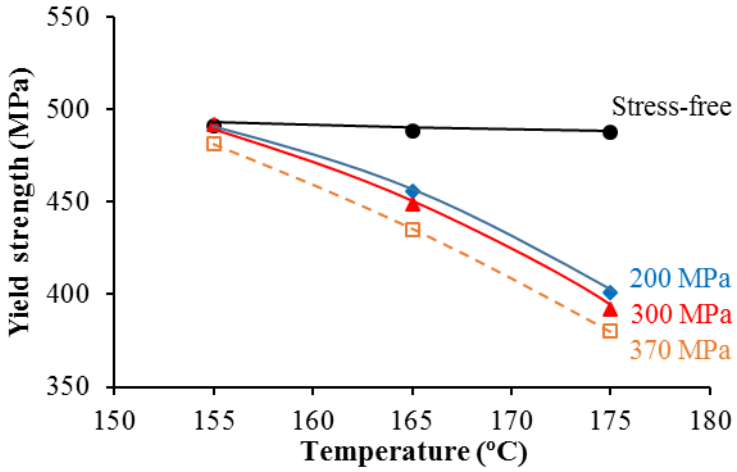
3.2.1 Yield strength

Fig. 5 shows the room-temperature yield strength (0.2% proof stress) of AA7B04-P after SRA tests with different durations, obtained through interrupted tests. As the as-received AA7B04-P is in an under-aged condition (artificially aged at 115 °C for 8 h, with a yield strength of 506 MPa), a subsequent artificial ageing would further strengthen the material. As shown in Fig. 5(a), the yield strength increases in the first few hours during stress-free ageing at 165 ºC and appears to achieve the peak-ageing state at around 4 h, with a yield strength of 516 MPa. Further ageing leads to the softening of the material, with a yield strength of 488 MPa at 16 h, indicating the occurrence of over-ageing. When the external stress was applied in the SRA tests at 165 ºC, the softening of the material (decrease of yield strength) is found after 2 h, indicating an accelerated ageing progress under external stresses during SRA tests. In addition, the loss in yield strength is more prominent under a larger applied stress, as shown in Fig. 5(a).

The yield strength results of the material after 16 h SRA tests under different initial stress levels and at different temperatures are plotted in Fig. 5(b). Under the stress-free condition, the yield strength experiences only a minor decrease with increasing temperature: 5 MPa reduction when the temperature increases from 155 °C to 175 °C. However, when the external stress is applied, the yield strength shows a significant decrease after SRA tests with increasing temperatures from 155 °C to 175 °C, about 90 and 110 MPa reduction under external stresses of 200 MPa and 370 MPa respectively. The phenomenon is related to the larger creep strains generated at higher temperatures during SRA tests shown in Fig. 4(b) and will be discussed later.



(a)



(b)

Fig. 5. (a) Evolution of yield strength during SRA tests under indicated initial stress levels at 165 ºC; (b) Yield strength after 16 h SRA tests at different temperatures and initial stress levels (solid symbols: elastically loaded; hollow symbols: plastically loaded).

3.2.2 Strength loss percentage

A strength loss percentage variable ($P_{\Delta\sigma_y}$) is defined in this study to quantitatively show the softening level of the material after SRA tests with different temperatures and initial stress levels, as:

$$P_{\Delta\sigma_y} = \frac{\sigma_{y0}-\sigma_{yf}}{\sigma_{y0}} \quad (5)$$

where σ_{y0} is the yield strength of the as-received AA7B04-P (506 MPa), and σ_{yf} represents the yield strength of the material after SRA tests. Fig. 6 plots the $P_{\Delta\sigma_y}$ results after SRA tests

in this study. At 155 °C, $P_{\Delta\sigma_y}$ experiences a slight increase, from 3.5% to 4.9%, when the applied stress increases from 0 to the yield point ($\sigma_{0.01\%}$). When the temperature increases, a much more significant softening behaviour is observed after SRA tests. At 175 °C, the $P_{\Delta\sigma_y}$ value increases significantly from 3.9% to 22.8%, when the initial stress increases from 0 to $\sigma_{0.01\%}$. The different softening phenomena observed at different temperatures in the stress-free and stress ageing conditions in Fig. 6 may be related to the precipitation progress of the material at different temperatures during SRA and will be discussed in Section 4.1.

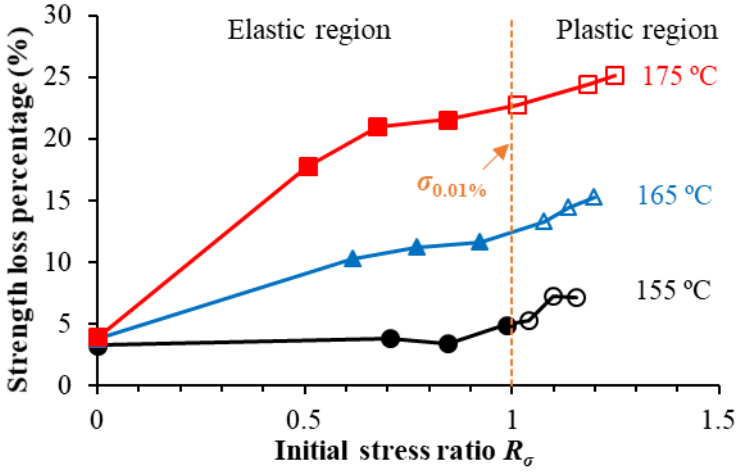
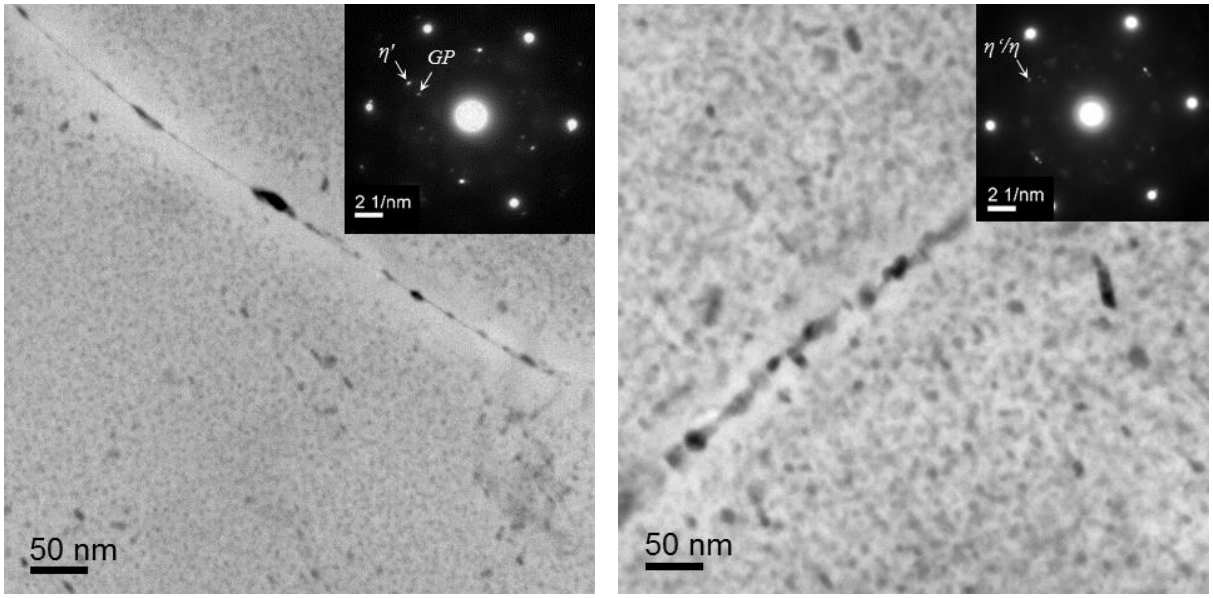


Fig. 6. Variations of strength loss percentage ($P_{\Delta\sigma_y}$) versus initial stress ratios ($R_\sigma = \sigma_{ini}/\sigma_{0.01\%}$) after 16 h SRA at indicated temperatures (solid symbols: elastically loaded; hollow symbols: plastically loaded).

3.3 Microstructures

Fig. 7 shows the TEM images of the as-received AA7B04-P and the 165 °C/16 h stress-free aged alloy. In the as-received material, small platelet precipitates are distributed homogenously within the grains, mainly consisting of GP zones and η' precipitates according to the selected area diffraction (SAD) pattern shown in Fig. 7(a), with an average precipitate radius (r_p) of 4.5 ± 2.3 nm. After 16 h stress-free ageing at 165 °C, the precipitates grow coarser (r_p = 8.9 ± 2.6 nm) and mainly consist of η' and η phases. Some rod-shaped η precipitates with larger sizes are also formed, as shown in Fig. 7(b), with an average length (l_r) of 15.7 ± 4.3 nm. These coarsened precipitates lead to the softening of the alloy, as shown in Fig. 5(a).



(a) (b)

Fig. 7. TEM images and SAD patterns showing the distribution of precipitates in (a) the as-received and (b) 165 ºC/16 h stress-free aged AA7B04-P.

TEM images of the 165 °C/16 h SRAed AA7B04-P samples under 300 MPa (elastic region) and 370 MPa (plastic region) are shown in Fig. 8. The precipitate types are the same as those in the stress-free aged sample in Fig. 7(b), but precipitates with larger sizes are found in the SRAed samples, as summarised in Table 3. These coarser precipitates then lead to the more significant softening of the SRAed material than that in the stress-free aged condition, as shown in Fig. 5(a). In addition, higher initial stress levels lead to coarser precipitates, especially in the plastic region. For example, about 0.4 nm increase of r_p is observed when the applied stress increases from 200 to 300 MPa in the elastic region, while the increase becomes 2.5 nm from 300 to 370 MPa in the plastic region, as listed in Table 3. Meanwhile, a higher fraction of much larger rod-shaped η precipitates has been formed in the SRAed sample when the initial stress is in the plastic region, as shown in Table 3 and Fig. 8.

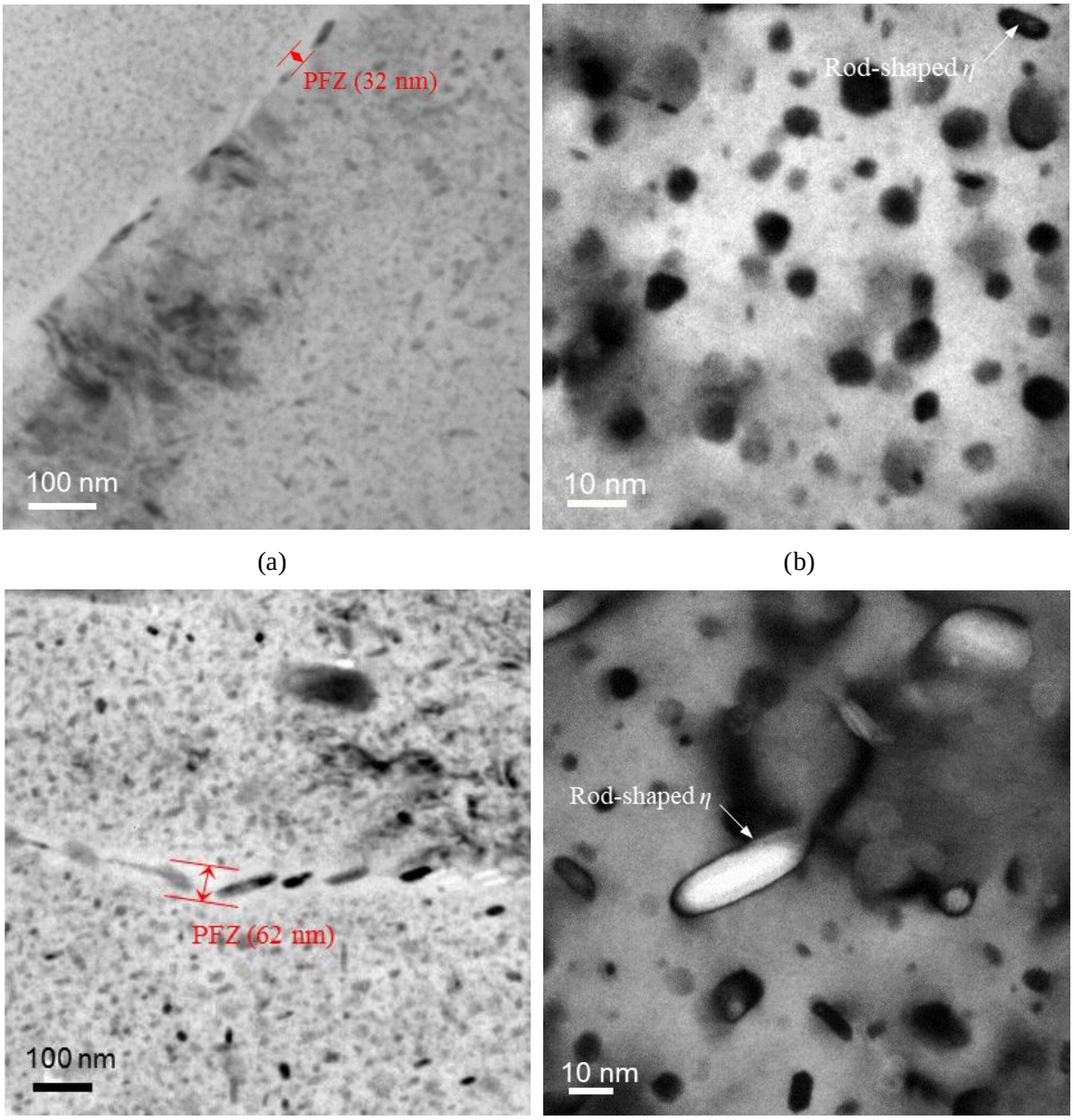
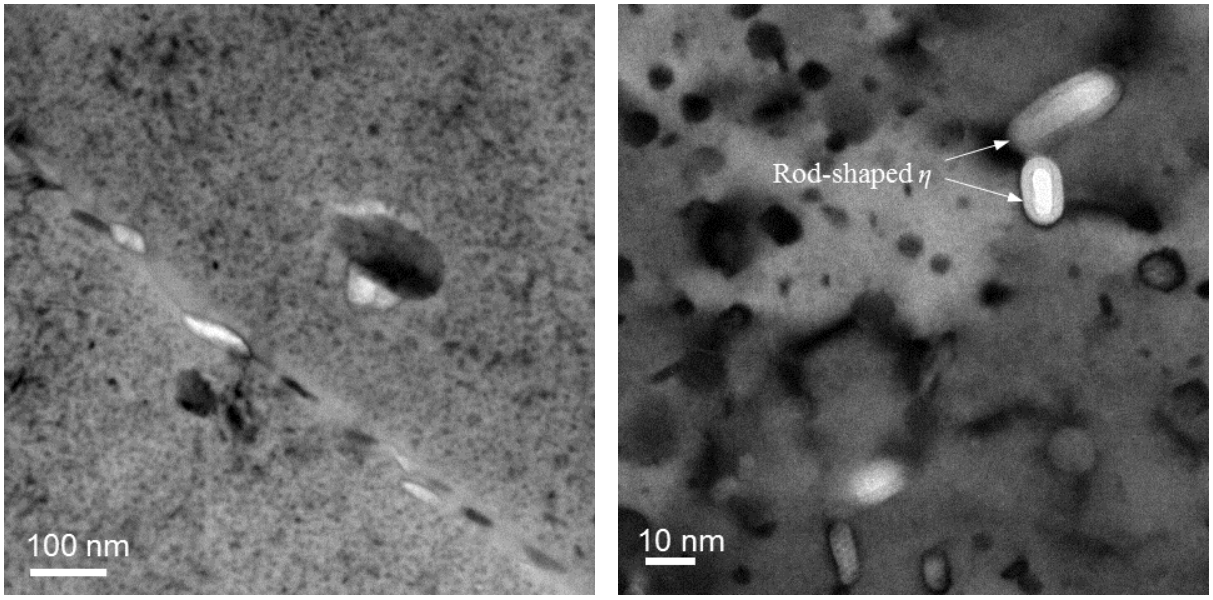


Fig. 8. TEM images with low and high magnifications showing the platelet and rod-shaped precipitates in 165 ºC/16 h SRAed AA7B04-P under the initial stress of: (a), (b) 300 MPa; (c), (d) 370 MPa.

Table 3. Dimensions of precipitates in the samples under different SRA conditions.

Sample	**As-received**	**Stress relaxation aged for 16 h**					
Temperature	-	165 °C				155 °C	175 °C
Stress (MPa)	-	0	200	300	370	370	370
r_p (nm)	4.5 ± 2.3	8.9 ± 2.6	9.8 ± 3.1	10.2 ± 3.5	12.7 ± 3.3	9.88 ± 3.1	13.3 ± 4.7
l_r (nm)	-	15.7 ± 4.3	18.2 ± 3.7	18.9 ± 4.2	25.1 ± 5.5	24.8 ± 4.3	36.7 ± 9.7
PFZ (nm)	-	23	26	32	62	52	80

Fig. 9 shows representative images taken from the sample after 165 °C/2 h SRA tests under 370 MPa. It is shown that the large rod-shaped η precipitates, which have been found in the 16 h SRAed sample in Fig. 8(d), were already formed after 2 h SRA tests in the plastic region, while only some small rod-shaped η precipitates are present in the sample under 300 MPa in the elastic region. Hence, the results indicate that the initial dislocations introduced by plastic loading can significantly facilitate and accelerate the formation and growth of rod-shaped η precipitates in the material.



(a) (b)

Fig. 9. TEM images with (a) low and (b) high magnifications showing precipitates distribution in the 165 °C/370 MPa SRAed AA7B04-P for 2 h.

Fig. 10 shows the TEM images of the 16 h/370 MPa SRAed samples at different temperatures. The measured dimensions of the precipitates in the tested samples are also summarised in Table 3. After 155 °C/16 h SRA, both η' and η precipitates can be found in the grains of the material, with a small fraction of rod-shaped η precipitates. Both the precipitate sizes and distributions are similar to those in the stress-free aged sample at 165 °C shown in Fig. 7(b), and hence, only a slight difference is shown in the yield strength of the two test conditions in Fig. 5(b). When the temperature increases to 175 °C, much larger precipitates are present in the grains of the material in Figs. 10(c) and 10(d). Meanwhile, a wider precipitate free zone (PFZ) is formed in the samples after SRA tests at a higher temperature, whose width is about 52, 62 and 80 nm respectively for the 16 h SRAed samples at 155, 165 and 175 °C, as listed in Table 3.

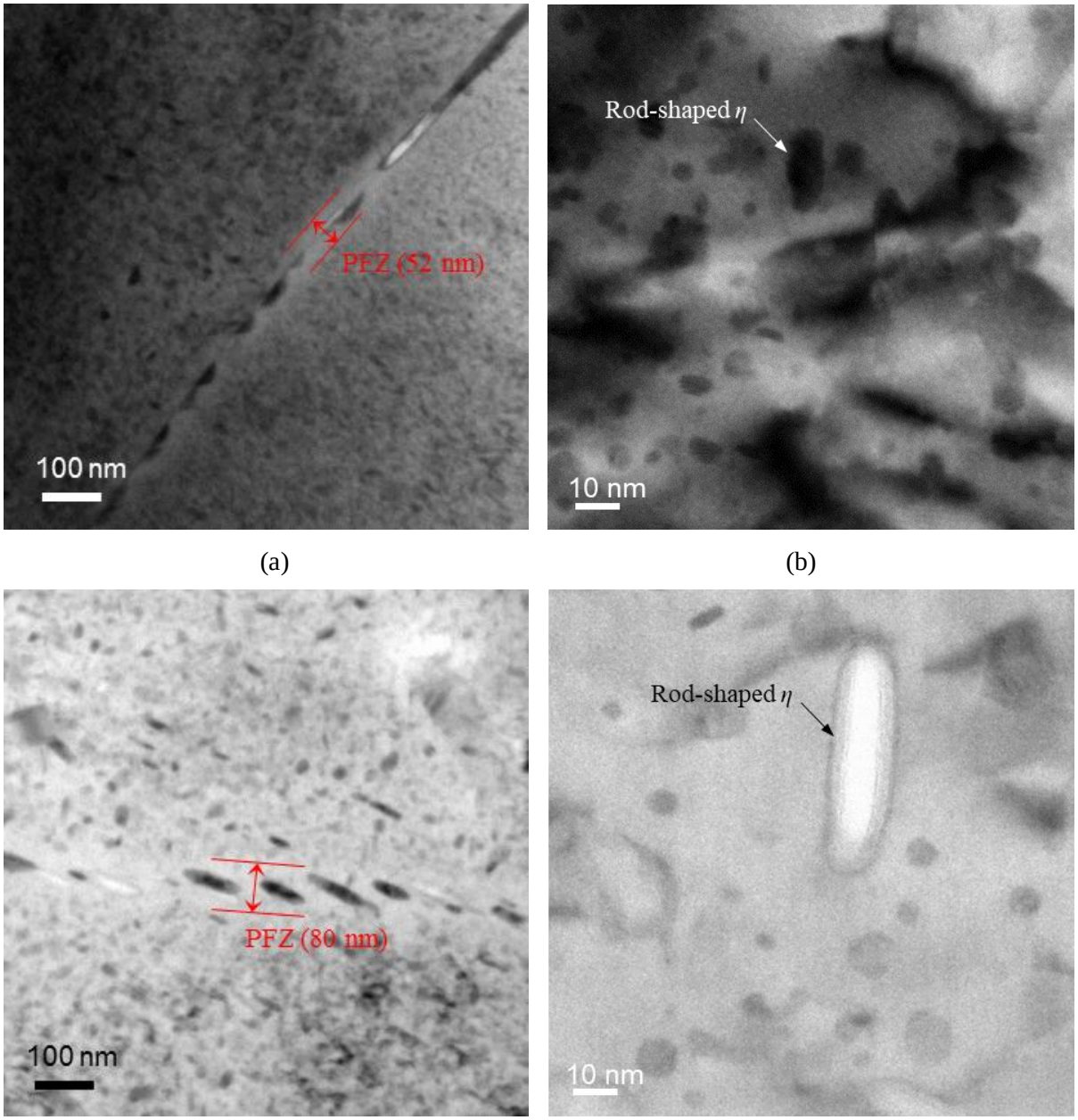


Fig. 10. TEM images showing the platelet and rod-shaped precipitates in 16 h/370 MPa SRAed AA7B04-P at the temperature of (a), (b) 155 °C; and (c), (d) 175 °C.

4. Discussion

4.1 Dependence of yield strength on stress and temperature

The yield strength of heat-treatable aluminium alloys is mainly comprised of its intrinsic strength and strength contributions from solid solutes, precipitates and dislocations [27]. Growth and coarsening of existing GP zones and η' precipitates and the formation of equilibrium η precipitates have been observed after stress-free ageing of AA7B04-P at 165 °C for 16 h, leading to the over-aged behaviour with a decreased precipitation hardening effect.

Meanwhile, the solid solution hardening is expected to decrease to a stable level due to the depleted free solid solutes in the matrix after precipitation. Hence, both effects contribute to an overall yield strength loss of about 20 MPa compared with the as-received material in Fig. 5(a).

It has been noticed that the external elastic stress applied during SRA tests can accelerate the growth and coarsening of precipitates due to the creep induced dislocations [28], and leads to larger precipitates (both platelet ones and rod-shaped ones) in the SRAed material than that with stress-free aged conditions, as shown in Fig. 7(b) and Fig. 8. Although the creep induced dislocations could enhance the yield strength through dislocation hardening effect, the softening effect from the coarsening of precipitates may play the dominant role during SRA, and thus leading to the accelerated over-ageing behaviour under higher stress levels in Fig. 5(a) and the larger loss of yield strength in the over-aged material with a higher applied stress after 165 °C/16 h SRA tests in Fig. 6. When loaded in the plastic region, initial dislocations are introduced into the material, which further accelerates the growth and coarsening of GP zones and η' precipitates, as shown in the TEM images in Fig. 8. In addition, it has been reported that dislocations can provide high energy sites for precipitation [29] and the dislocations introduced by plastic loading have led to the accelerated formation of much larger rod-shaped η precipitates in the SRAed AA7B04-P samples in the plastic region in this study, as demonstrated in Fig. 8(d) and Fig. 9(b). With the combined effects of accelerated coarsening of existing η' precipitates and formation of larger rod-shaped η precipitates in the material from the initial dislocations introduced by plastic loading, over-ageing behaviour occurs much earlier during SRA tests and more significant yield strength loss of the over-aged material was observed in Fig. 6 after 16 h SRA tests in the plastic region than that in the elastic region.

Temperature can directly determines the precipitate types and distributions in aluminium alloys during artificial ageing [30]. The temperature range investigated in this study is comparatively small, from 155 to 175 °C, which are potential temperatures for CAF applications of this alloy, and the precipitate types are not affected by the temperatures used, as observed in Section 3.3. However, increasing temperature can accelerate the growth and coarsening of precipitates, and also facilitate the nucleation and growth of heterogeneous precipitates [31], leading to the larger η' precipitates with higher fraction of rod-shaped η precipitates and the larger PFZ zones in the over-aged material after SRA tests, as shown in Figs. 8 and 9. Meanwhile, higher temperature could facilitate the dislocation recovery process [28], leading to a lower dislocation hardening effect in the material. Both phenomena contribute

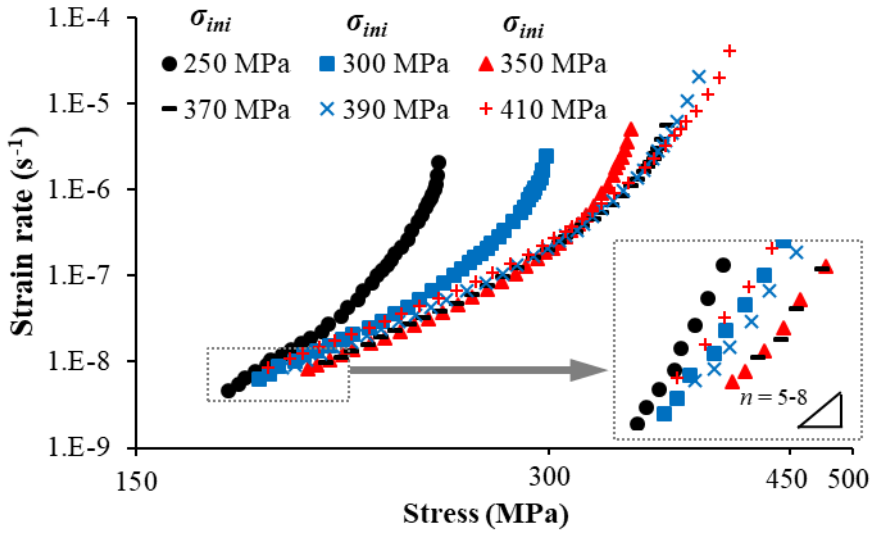
to the much more significant softening of the material after SRA with the same initial stress level at higher temperatures, as shown in Fig. 6.

4.2 Dependence of stress relaxation on stress and temperature

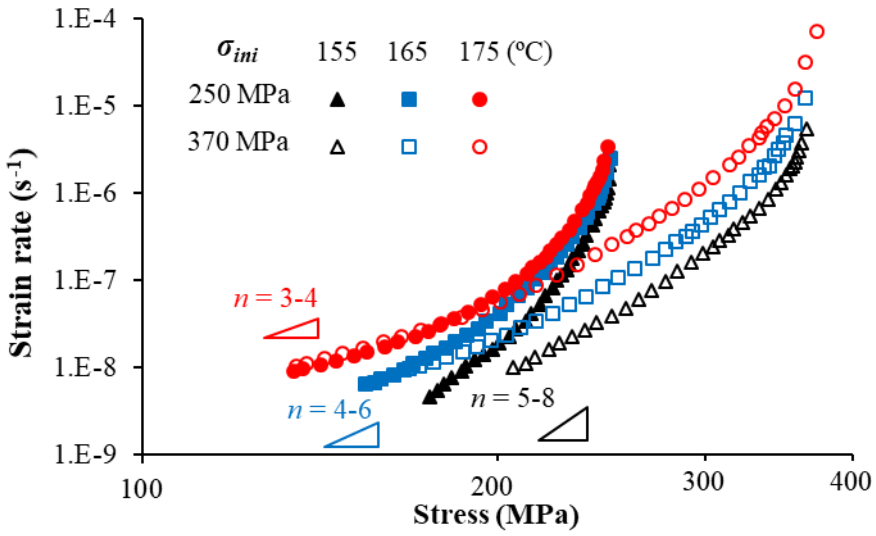
It is known that the stress relaxation is generated mainly due to the occurrence of creep deformation during SRA tests, and thus, the creep mechanisms can be used to analyse the stress relaxation behaviour [9, 18]. Creep stress exponent *n* is a parameter commonly used to characterise the detailed creep mechanisms at the steady-state stage, which can be calculated by [32]:

$$n = \frac{\partial ln\dot{\varepsilon}_{cm}}{\partial ln\sigma} \quad (6)$$

where $\dot{\varepsilon}_{cm}$ is the creep strain rate at the steady-state creep stage. The variations of the creep strain rate data with the changing stresses during SRA tests under different initial stress levels and temperatures are plotted in Fig. 11, and the *n* values obtained by the data at the final period of SRA tests, during which the steady-state creep stage is generally expected (with $\dot{\varepsilon}_c < 10^{-8}$ s^{-1}), are also plotted in the figures. It is well known that a stress exponent $n = 4 – 9$ generally indicates the dislocation creep mechanism [18]. The *n* values obtained under different stress levels at the three test temperatures are all located in the range of dislocation creep mechanism, as shown in Fig. 11 ($n = 5 – 8$ at 155 °C, $n = 4 – 6$ at 165 °C and $n = 3 – 4$ at 175 °C). The same mechanism controlling stress relaxation at the three test temperatures leads to the similar trend of maximum stress drop ($\Delta\sigma_{max}$) at different temperatures, as shown in Fig. 3. In addition, it has been reported that a higher temperature can provide more energy for the dislocation propagation during creep, leading to easier dislocation movements and lower threshold stresses for creep of the materials [33]. The lower threshold stress of the material at higher temperatures then lead to the more significant stress relaxation behaviour with larger $\Delta\sigma_{max}$ values at the same stress level shown in Figs. 2 and 3.



(a)



(b)

Fig. 11. Creep strain rate variations during SRA tests: (a) under different initial stress levels at 155 °C and (b) under 250 and 370 MPa at different temperatures.

Achieving the highest creep strains for plastic deformation with a minimum loss of yield strength is an ideal condition for materials after CAF process. The relationship between the creep strains and the yield strength loss percentage of the material after 16 h SRA tests at the three test temperatures are plotted in Fig. 12. It can be seen that the creep strains experience only a slight increase with increasing temperature at a similar loading condition, e.g., creep strain only increases from 0.250% to 0.255% at the strain ratio R_ε = 1.1 when the temperature increases from 155 to 175 °C. However, a significant difference in yield strength loss percentage is observed at the same conditions, e.g., $P_{\Delta\sigma_y}$ increases from 5.2% to 22.8% for the

same conditions above. Hence, it is reasonable to conclude that the yield strength has a much higher sensitivity to the temperatures than the creep strains during SRA tests, and a temperature below 165 °C is suggested for CAF of AA7B04-P, so that a high stress relaxation level can be obtained with a strength loss less than 15% after 16 h forming, as indicated in Fig. 12.

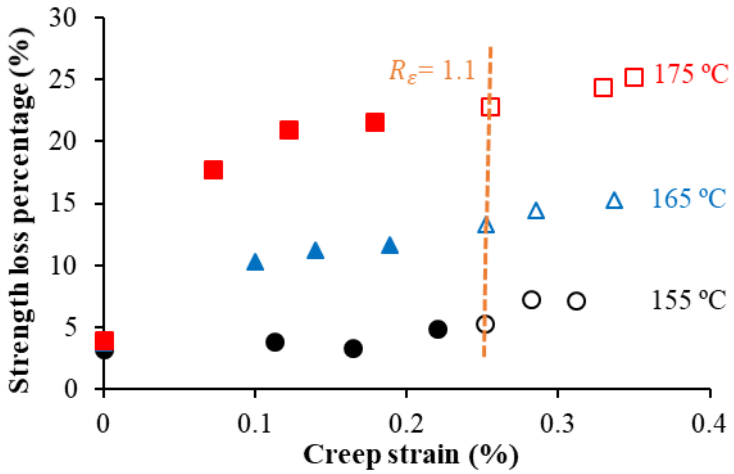


Fig. 12. Relationship between the accumulated creep strains and the yield strength loss percentage in the material after 16 h SRA tests at indicated temperatures (solid symbols: elastically loaded; hollow symbols: plastically loaded).

5. Conclusions

The stress and temperature dependence of the SRA behaviour of an Al-Zn-Mg alloy, AA7B04-P, has been comprehensively investigated through both SRA and tensile tests at three temperatures (155, 165 and 175 °C) and under various initial stress levels in both elastic and plastic regions. TEM observations of some selected samples have also been performed for detailed analysis and discussion. The following conclusions can be drawn:

a) Initial dislocations generated during loading significantly change the stress relaxation behaviour of the material. The 0.01% offset stress is shown in this study to be a better and appropriate choice to divide the elastic and plastic loading conditions for SRA behaviour, with which a linear relationship between the maximum stress drop after SRA tests and the applied stress ratio (or strain ratio) exists in the elastic region, irrespectively of test temperatures.

b) Dislocation creep mechanism plays the dominant role in stress relaxation of the alloy at the investigated stresses and temperatures, with the stress exponent n ranging from 3 to 8. n value decreases with increasing temperature. In addition, a lower creep threshold stress at a higher SRA temperature leads to larger stress relaxation levels, e.g., the maximum stress drop

after 16 h/370 MPa SRA tests increases from 173 to 239 MPa when the temperature increases from 155 to 175 ℃.

c) A more significant loss of yield strength occurs after SRA tests in the plastic region, due to the combined effect of accelerated growth and coarsening of η' precipitates from higher external stresses and formation of large rod-shaped η precipitates by initial dislocations from plastic loading. Meanwhile, the larger precipitates and wider precipitate free zones in the over-aged material after SRA tests at higher temperatures lead to more significant yield strength loss.

d) The yield strength has a much higher sensitivity to the temperature during SRA tests than the creep strain has. For CAF application of AA7B04-P, a processing temperature below 165 ℃ is recommended, so that large creep strains can be generated with the strength loss less than 15% after 16 h forming.

Declarations of interest: none.

Acknowledgements

The strong support from the Aviation Industry Corporation of China (AVIC) Manufacturing Technology Institute (MTI) for this funded research is much appreciated. The research was performed at the AVIC Centre for Structural Design and Manufacture at Imperial College London.

References

[1] A. Heinz, A. Haszler, C. Keidel, S. Moldenhauer, R. Benedictus, W. Miller, Recent development in aluminium alloys for aerospace applications, Materials Science and Engineering: A 280(1) (2000) 102-107.

[2] Y. Li, Z. Shi, J. Lin, Y.-L. Yang, P. Saillard, R. Said, Effect of machining-induced residual stress on springback of creep age formed AA2050 plates with asymmetric creep-ageing behaviour, International Journal of Machine Tools and Manufacture 132 (2018) 113-122.

[3] T. Dursun, C. Soutis, Recent developments in advanced aircraft aluminium alloys, Materials & Design (1980-2015) 56 (2014) 862-871.

[4] A.C. Lam, Z. Shi, H. Yang, L. Wan, C.M. Davies, J. Lin, S. Zhou, Creep-age forming AA2219 plates with different stiffener designs and pre-form age conditions: Experimental and finite element studies, Journal of Materials Processing Technology 219 (2015) 155-163.

[5] M.C. Holman, Autoclave age forming large aluminum aircraft panels, Journal of Mechanical Working Technology 20 (1989) 477-488.

[6] Y. Xu, L. Zhan, M. Huang, R. Shen, Z. Ma, L. Xu, K. Wang, X. Wang, Deformation behavior of Al-cu-mg alloy during non-isothermal creep age forming process, Journal of Materials Processing Technology 255 (2018) 26-34.

[7] K. Ho, J. Lin, T. Dean, Constitutive modelling of primary creep for age forming an aluminium alloy, Journal of Materials Processing Technology 153 (2004) 122-127.

[8] F. Lyu, Y. Li, X. Huang, Z. Shi, Y. Zeng, J. Lin, An investigation of creep age forming of AA7B04 stiffened plates: Experiment and FE modelling, Journal of Manufacturing Processes 37 (2019) 232-241.

[9] L. Zhan, J. Lin, T. Dean, A review of the development of creep age forming: Experimentation, modelling and applications, International Journal of Machine Tools and Manufacture 51(1) (2011) 1-17.

[10] X.Y. Liu, Q.L. Pan, X.L. Zhang, S.X. Liang, F. Gao, L.Y. Zheng, M.X. Li, Creep behavior and microstructural evolution of deformed Al–Cu–Mg–Ag heat resistant alloy, Materials Science and Engineering: A 599 (2014) 160-165.

[11] C. Lei, H. Yang, H. Li, N. Shi, L. Zhan, Dependences of microstructures and properties on initial tempers of creep aged 7050 aluminum alloy, Journal of Materials Processing Technology 239 (2017) 125-132.

[12] Y. Li, Z. Shi, J. Lin, Y.-L. Yang, B.-M. Huang, T.-F. Chung, J.-R. Yang, Experimental investigation of tension and compression creep-ageing behaviour of AA2050 with different initial tempers, Materials Science and Engineering: A 657 (2016) 299-308.

[13] J. Zhang, Y. Deng, X. Zhang, Constitutive modeling for creep age forming of heat-treatable strengthening aluminum alloys containing plate or rod shaped precipitates, Materials Science and Engineering: A 563 (2013) 8-15.

[14] H. Chandler, A comparison between steady state creep and stress relaxation in copper, Materials Science and Engineering: A 527(23) (2010) 6219-6223.

[15] Y. Li, Z. Shi, J. Lin, Y.-L. Yang, P. Saillard, R. Said, FE simulation of asymmetric creep-ageing behaviour of AA2050 and its application to creep age forming, International Journal of Mechanical Sciences 140 (2018) 228-240.

[16] Y. Yang, L. Zhan, R. Shen, J. Liu, X. Li, M. Huang, D. He, Z. Chang, Y. Ma, L. Wan, Investigation on the creep-age forming of an integrally-stiffened AA2219 alloy plate: experiment and modeling, The International Journal of Advanced Manufacturing Technology 95(5-8) (2018) 2015-2025.

[17] F. Eberl, S. Gardiner, G. Campanile, G. Surdon, M. Venmans, P. Prangnell, Ageformable panels for commercial aircraft, Proceedings of the Institution of Mechanical Engineers, Part G: Journal of Aerospace Engineering 222(6) (2008) 873-886.

[18] J. Chen, J. Jiang, L. Zhen, W. Shao, Stress relaxation behavior of an Al–Zn–Mg–Cu alloy in simulated age-forming process, Journal of Materials Processing Technology 214(4) (2014) 775-783.

[19] L. Zhan, Z. Ma, J. Zhang, J. Tan, Z. Yang, H. Li, Stress relaxation ageing behaviour and constitutive modelling of a 2219 aluminium alloy under the effect of an electric pulse, Journal of Alloys and Compounds 679 (2016) 316-323.

[20] Q. Rong, Y. Li, Z. Shi, L. Meng, X. Sun, X. Sun, J. Lin, Experimental investigations of stress-relaxation ageing behaviour of AA6082, Materials Science and Engineering: A 750 (2019) 108-116.

[21] R.A. Jeshvaghani, M. Emami, H. Shahverdi, S. Hadavi, Effects of time and temperature on the creep forming of 7075 aluminum alloy: Springback and mechanical properties, Materials Science and Engineering: A 528(29-30) (2011) 8795-8799.

[22] Y. Lin, Y.-C. Xia, Y.-Q. Jiang, L.-T. Li, Precipitation in Al–Cu–Mg alloy during creep exposure, Materials Science and Engineering: A 556 (2012) 796-800.

[23] R.A. Jeshvaghani, H. Zohdi, H. Shahverdi, M. Bozorg, S. Hadavi, Influence of multi-step heat treatments in creep age forming of 7075 aluminum alloy: Optimization for springback, strength and exfoliation corrosion, Materials characterization 73 (2012) 8-15.

[24] P. Juijerm, I. Altenberger, Residual stress relaxation of deep-rolled Al–Mg–Si–Cu alloy during cyclic loading at elevated temperatures, Scripta Materialia 55(12) (2006) 1111-1114.

[25] G. Lloyd, J. Martin, The effect of dislocation density on the creep of dispersion-strengthened copper crystals, Materials Science and Engineering 46(1) (1980) 1-13.

[26] M.E. Kassner, Chapter 2 - Five-Power-Law Creep, in: M.E. Kassner (Ed.), Fundamentals of Creep in Metals and Alloys (Third Edition), Butterworth-Heinemann, Boston, 2015, pp. 7-102.

[27] Y. Li, Z. Shi, J. Lin, Y.-L. Yang, Q. Rong, B.-M. Huang, T.-F. Chung, C.-S. Tsao, J.-R. Yang, D.S. Balint, A unified constitutive model for asymmetric tension and compression creep-ageing behaviour of naturally aged Al-Cu-Li alloy, International Journal of Plasticity 89 (2017) 130-149.

[28] J.-H. Zheng, R. Pan, C. Li, W. Zhang, J. Lin, C.M. Davies, Experimental investigation of multi-step stress-relaxation-ageing of 7050 aluminium alloy for different pre-strained conditions, Materials Science and Engineering: A 710 (2018) 111-120.

[29] A. Deschamps, F. Livet, Y. Brechet, Influence of predeformation on ageing in an Al–Zn–Mg alloy—I. Microstructure evolution and mechanical properties, Acta materialia 47(1) (1998) 281-292.

[30] T. Dorin, A. Deschamps, F. De Geuser, C. Sigli, Quantification and modelling of the microstructure/strength relationship by tailoring the morphological parameters of the T1 phase in an Al–Cu–Li alloy, Acta materialia 75 (2014) 134-146.

[31] S. Wang, M. Starink, Precipitates and intermetallic phases in precipitation hardening Al–Cu–Mg–(Li) based alloys, International Materials Reviews 50(4) (2005) 193-215.

[32] M. Mostafa, G. Al-Ganainy, A.A. El-Khalek, R. Nada, Steady-state creep and creep recovery during transformation in Al–Zn alloys, Physica B: Condensed Matter 336(3-4) (2003) 402-409.

[33] C.A.P. Horton, A temperature dependent ‘threshold’ stress for grain boundary sliding, Scripta Metallurgica 8(1) (1974) 1-6.